

Stage III Annealing Study of Electron-Irradiated Pure Aluminum*

Y. N. LWIN† AND M. DOYAMA

Argonne National Laboratory, Argonne, Illinois

AND

J. S. KOEHLER

Materials Research Laboratory and the Department of Physics, University of Illinois, Urbana, Illinois

(Received 18 August 1967)

Pure aluminum was irradiated at about 90°K using 2-MeV electrons. Isochronal and isothermal annealing studies were carried out. The isochronal anneals were for 10 and 30 min at temperatures 10°C apart. The isothermals were for 64 min at temperatures 20°C apart. The major results were: Stage III occurs by a second-order process with activation energy $E_{III} = 0.62 \pm 0.04$ eV. From the fact that this activation energy agrees well with that observed after quenching, it is concluded that stage III in aluminum occurs by vacancy migration.

I. INTRODUCTION

THE recovery of electrical resistivity changes in pure Al and Al alloys following neutron and electron irradiation at liquid-nitrogen temperature has been studied by several investigators.¹⁻⁹

Federighi *et al.*¹⁻⁴ in a series of experiments irradiated pure Al and Al alloys with neutrons. Recovery spectra in the Stage II and Stage III regions were investigated. They attribute the recovery in Stage III to the migration of single vacancies to interstitial clusters formed at the irradiation temperature. They measured an activation energy of 0.61 ± 0.03 eV for pure Al during Stage III recovery.

Frois and Dimitrov^{5,6} have reported the recovery of pure Al after neutron irradiation at liquid-nitrogen temperatures. They obtained an activation energy of 0.56 ± 0.06 eV for Stage III recovery. McReynolds *et al.*⁹ in their early investigation of neutron irradiation effects in Cu and Al at liquid-nitrogen temperature obtained an activation energy of about 0.55 eV for Stage III recovery in Al.

Sosin *et al.*⁸ observed Stage III recovery after electron irradiation in pure Al with an activation energy of 0.45 ± 0.01 eV.

It appears that there is a reasonable agreement in the experimental results of neutron bombardment by different investigators. The above experiments show a different activation energy for Stage III after electron irradiation than that seen after neutron irradiation.

The present research was carried out to understand Stage III annealing. We shall attempt to check the following points:

- (a) to obtain accurate activation energies for Stage III by different methods;
- (b) to obtain kinetics and activation energy spectra in Stage III; and
- (c) to decide whether the difference in E_m^{III} found using neutron and electron irradiation is real.

II. EXPERIMENTAL PROCEDURES

A. Cryostat

The liquid-nitrogen cryostat used, Fig. 1, is similar to the one described by Dworschak, Herschbach, and Witt¹⁰ designed for heavy-particle bombardment. For the present work a new cryostat was constructed with the following modifications. To improve the precision of electron flux measurements, the beam passage dimensions were enlarged so that it permits the mounting of a Faraday cage behind the specimen block. The cage collects the electron beam after striking the samples; it is separated from the samples only by a 1-mil aluminum window. The cage was electrically insulated from the main cryostat and it was in vacuum. Overheating of this cage by long exposure of electron beam was overcome by mounting the cage on a piece of solid boron nitride, which conducts away the heat to the outside portions of the cryostat. All flanges in this cryostat are sealed with indium O rings. The vacuum inside the beam passage can be maintained better than 10^{-4} mm of Hg during irradiation, thus reducing the gas scattering of the electron beam.

* Based on work performed under the auspices of the U. S. Atomic Energy Commission. This paper is based on a thesis submitted by Y. N. Lwin in partial fulfillment of the requirements for the Ph.D. in nuclear engineering at the University of Illinois.

† Present address: Department of Physics, Western Illinois University, Macomb, Ill.

¹ S. Ceresara, T. Federighi, D. Gelli, and F. Pieragostini, *Nuovo Cimento* **29**, No. 6, 1244 (1963).

² S. Ceresara, T. Federighi, and F. Pieragostini, *Phys. Letters* **6**, 152 (1963).

³ S. Ceresara, H. Elkholy, T. Federighi, and F. Pieragostini, *Phys. Letters* **16**, 9 (1965).

⁴ T. Federighi, S. Ceresara, and F. Pieragostini, *Phil. Mag.* **12**, 1093 (1965).

⁵ C. Frois and O. Dimitrov, *Journées Soc. Française Metall.*, **12** (1964).

⁶ C. Frois and O. Dimitrov, *Compt. Rend.* **258**, 5647 (1964).

⁷ C. Budin and P. Lucasson, *Phys. Letters* **16**, 229 (1965).

⁸ A. Sosin and L. H. Rachal, *Phys. Rev.* **130**, 2238 (1963).

⁹ A. W. McReynolds, W. Augustyniak, M. McKeown, and D. B. Rosenblatt, *Phys. Rev.* **98**, 418 (1955).

¹⁰ F. Dworschak, K. Herschbach, and F. Witt, *Rev. Sci. Instr.* **35**, 46 (1964).

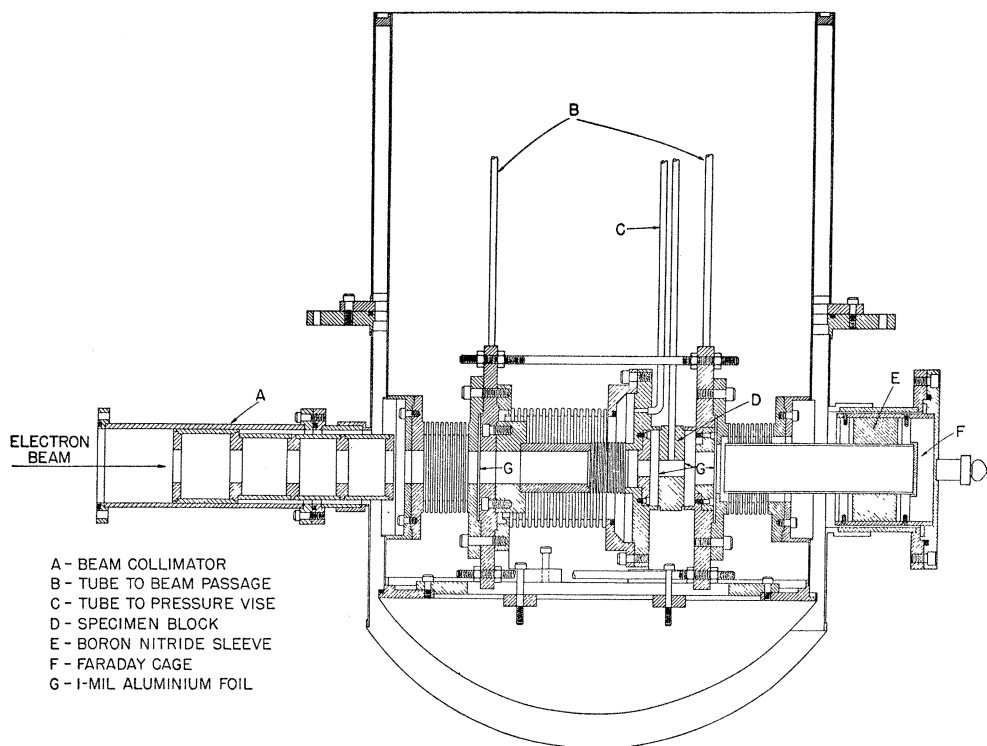


FIG. 1. Liquid-nitrogen cryostat.

B. Specimen Preparation and Mounting

The pure Al specimens used in this experiment were of two types. In one type, the starting material was 40 mil, 69 grade zone-refined aluminum supplied by Cominco. We drew this wire to 5-mil diameter using diamond dies. The wire was etched with a hot mixture of 95% phosphoric acid and 5% nitric acid between drawings. The specimens were mounted in the manner described by Dworschak *et al.*^{11,12} The residual resistivity of a mounted specimen after an anneal was about $1.5 \times 10^{-9} \Omega \text{ cm}$. Some of the specimens mounted in this manner were apparently in poor contact with the frames after the anneal due to difficulty in spot-welding 5-mil Al wire to an Al frame made from 5-mil foils.

In another type, the starting material was an ingot of zone-refined aluminum supplied by Cominco. This was cut into strips of 35–40 mil. The strips were rolled down to 5-mil foils from which the specimens were cut out by hand to the shape shown in Fig. 2. Before annealing the specimens were etched with boiling HNO_3 and HCl and with acetone. All pure Al specimens were annealed in vacuum (better than $5 \times 10^{-6} \text{ mm Hg}$) for 3 h at 450°C .

This type of mounting made it possible to handle the specimens after annealing with a minimum of cold

¹¹ F. Dworschak and J. S. Koehler, *Phys. Rev.* **140**, A941 (1965).

¹² F. Dworschak, K. Herschbach, and J. S. Koehler, *Phys. Rev.* **133**, A293 (1963).

work. Since the current leads and potential leads are part of the specimen itself without requiring spot welding, there was no problem of losing electrical contact. The ratio $\rho_{20^\circ\text{C}}/\rho_{4.2^\circ\text{K}}$ was about 2700 for all strip specimens prepared in this way.

C. Irradiation Procedure

The Van de Graaff machine of the Material Research Laboratory at the University of Illinois was used for the present experiment. The cryostat was visually aligned with respect to the 90° electron beam. The beam uniformity was checked by irradiating a glass slide mounted on a dummy block with a short pulse (a few seconds) of electrons. The uniformity in coloring on the glass slide gives a good indication of the uniformity of the beam. To monitor the temperature rise during irradiation and later in annealing, a copper-constantan thermocouple (2-mil diameter) attached to a dummy specimen was mounted in each block. Throughout the run, temperature was recorded by using a microvolt amplifier and recorder. The temperature response monitored on the dummy specimen during irradiation gave a very reliable and reproducible temperature control. The temperature variation followed exactly the variation of current from Faraday cage which was also monitored throughout. The energy of the electrons was well regulated (within 0.025 keV) at 2 MeV.

TABLE I. Summary of data for irradiated samples.

Specimen Block	Material and type	Dose (C)	Radiation-induced resistivity ($10^{-9} \Omega \text{ cm}$)	Treatment given	Resistivity before irradiation ($10^{-9} \Omega \text{ cm}$)
10 1	Al (foil)	0.027	0.19		0.98
10 2	Al (foil)		0.23		1.03
6 1	Al (foil)	0.17	0.76	Isothermal (20°C)	0.99
6 2	Al (foil)	0.17	0.82	(4, 4, 8, 16, 32 min)	1.04
1 1	Al (foil)	0.30	1.14	Isothermal (20°C)	1.00
1 2	Al (foil)		1.30	(4, 4, 8, 16, 32 min)	1.00
E 1	Al (foil)	0.50	1.44	Isothermal (-50°C) (500 min)	1.04
E 2	Al (foil)		1.61		1.01
A 21	Al (foil)	0.81	2.18	Isothermal (10 min) 10°C	0.96
A 22	Al (foil)		2.08		0.99
4 1	Al (foil)	1.0	2.29	Isothermal (-50°C)	1.00
4 2	Al (foil)	1.0	2.12		0.98
7 1	Al (foil)	1.0	2.27	Isothermal (10, 15 min) (Alternate Temp., -40°C and -50°C)	1.02
7 2	Al (foil)		2.48		1.01
B 1	Al (foil)	2.17	3.45	Isothermal (20°C)	0.99
B 2	Al (wire)		4.48	(4, 4, 8, 16, 32 min)	1.52
D 1	Al (wire)	1.0	3.31	Isothermal (20°C)	1.65
				(4, 4, 8, 16, 32 min)	1.65
2 2	Al (wire)	0.5	1.65	Isothermal (30 min) 10°C	1.56
5 1	Al (wire)	0.5	2.00	Isothermal (10 min) 10°C	1.66

The range of the particles of this energy in Al is approximately 140 mil, so that there should be no inhomogeneities in the samples due to the end of range effects in the samples. The electron beam passed through three windows of Al foil (a total of 3 mil) before striking the samples. The energy loss of 2 MeV electrons was estimated to be of about 60 keV. The effective incident energy at the samples was approximately 1.94 MeV.

Maximum current used was $10 \mu\text{A}/\text{cm}^2$ in one case, which gave a temperature rise of about 40°C above liquid- N_2 temperature. The average electron beam was maintained at about $7.5 \mu\text{A}/\text{cm}^2$ and the specimen temperature never exceeded 20°C above liquid N_2 temperature. For a constant value of Van de Graaff current the dummy temperature gradually rose during the course of the entire irradiation. This is attributed to a steady decrease of thermal conductivity of the irradiated samples as their resistance increases. All samples were stored in liquid nitrogen after irradiation until measurement.

The liquid-nitrogen consumption was about 25 liter per 3 h of irradiation time with a beam current of $7.5 \mu\text{A}/\text{cm}^2$.

D. Resistivity Measurement and Annealing

The resistance of all samples was measured at liquid-helium temperature. The method used was a standard potentiometric method. The current was determined from the voltage across a standard $1\text{-}\Omega$ resistance in series with the specimen. A Leeds and Northrup K-3

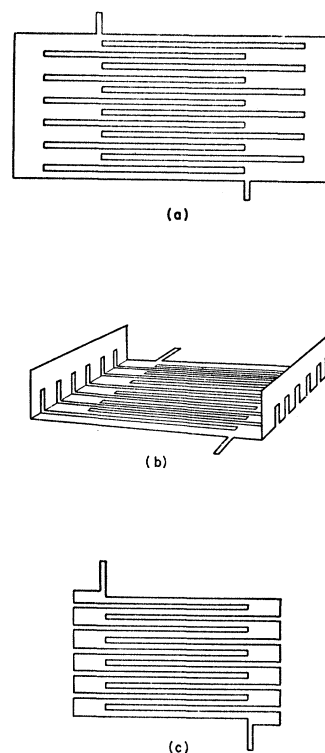


FIG. 2. Steps in preparing foil specimens: One first cuts the foil into shape (a). The end tabs are then bent up as in (b). The foil is then glued to the specimen mounting block and the end tabs are cut off leaving the sample as in (c) with the big end regions glued down. The irradiation damages the middle narrow portions of the specimen.

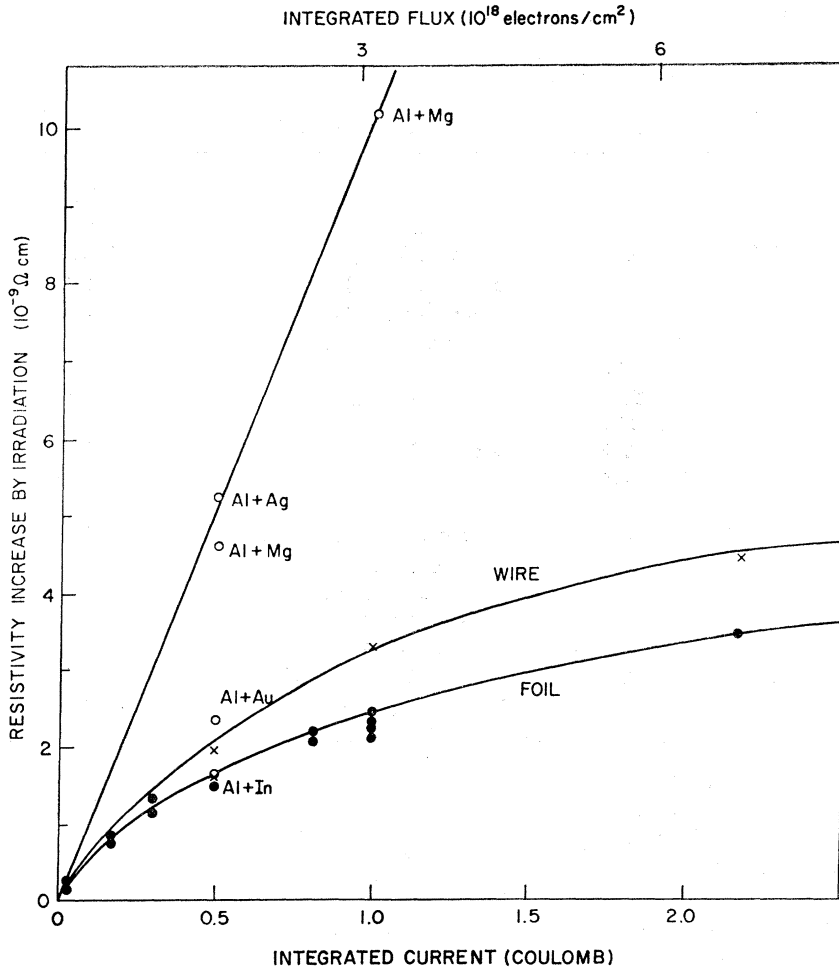


FIG. 3. Resistivity increase as a function of integrated electron flux for samples bombarded by 2-MeV electrons at 80°K.

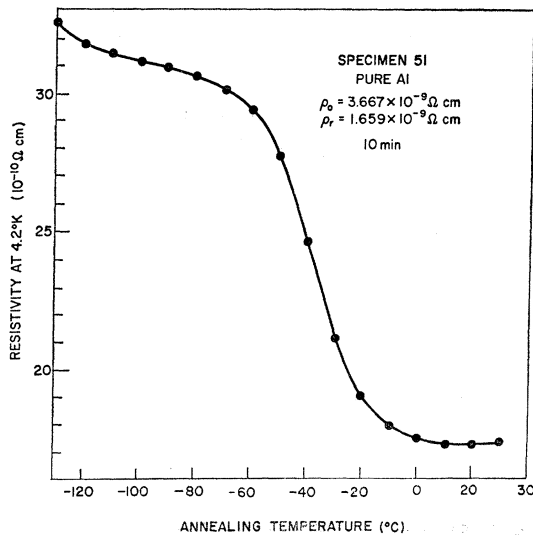
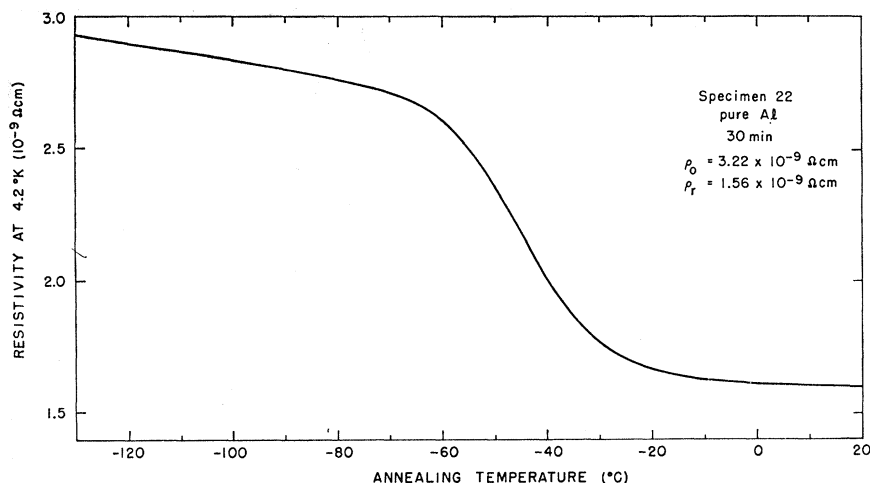


FIG. 4. Isochronal recovery of the electrical resistivity increase ($\Delta\rho$) for specimen (5-1) pure Al following electron irradiation near 80°K, and annealed for 10 min every 10°C. In Fig. 4 and in subsequent figures ρ_0 is the initial defect resistivity and ρ_r is the resistivity at 4.2°K before irradiation.

potentiometer and an electronic null detector were used. The voltage across the specimen was measured by a Rubicon thermofree microvolt potentiometer in conjunction with a Rubicon photoelectric galvanometer. The effect of stray thermal voltages in the potential leads was eliminated by reversing the current direction and taking the average of the readings for the two current directions.

Annealing treatments were carried out by transferring the block to a constant temperature bath cooled by liquid nitrogen. The bath and the liquid used have been described before.¹² Pure alcohol was used for temperatures above -20°C . The temperature of the bath was measured by a Leeds and Northrup platinum resistance thermometer calibrated by the National Bureau of Standards. The bath temperature was regulated by an electric heater and maintained constant to within $\pm 0.02^\circ\text{C}$. The difference in temperature between the dummy specimen and the bath was measured with a thermocouple attached to the dummy, the reference temperature being that of the bath. These readings were recorded during the warming up time until it

FIG. 5. Isochronal recovery of the electrical resistivity increase ($\Delta\rho$) for specimen (2-2) pure Al following electron irradiation near 80°K, and annealed for 30 min every 10°C.



reached equilibrium. Corrections to the annealing time were made as described by Grenning and Koehler.¹³

III. EXPERIMENTAL RESULTS

A total of 19 specimens, mounted on 11 different specimen blocks, were irradiated with 2-MeV electrons near liquid-nitrogen temperature in 11 different irradiation runs. Table I gives the composition of the specimens, the integrated flux used, the radiation-induced resistivity, and treatment after irradiation.

A. Damage Production

The plots of resistivity increase versus electron flux for Al are given in Fig. 3.

The experimental points were obtained from different specimen blocks which were irradiated to different fluxes in this experiment. The features to be noted are: (1) The resistivity increase $\Delta\rho$ versus the integrated flux for pure Al specimens deviated from linearity and this "bending over" is probably a result of Stage I annealing and (2) the downward curvature is more pronounced in the foil specimens of pure Al. These specimens have the highest purity. The wire specimens of pure Al, which contain higher background impurity than the foil specimens, show higher damage than the foil specimens.

B. Isochronal Annealing

Isochronal annealing treatments were given to three samples of pure Al. In one case the anneal was for 10 min every 10°C between -130 and 20°C. In another case the anneal was for 30 min every 10°C. These results are presented in Fig. 4 and 5, respectively. The experimental points are connected with a "smooth" curve. Each smooth segment between two experimental points was obtained from a seventh-order polynomial fitted

¹³ D. A. Grenning and J. S. Koehler, Phys. Rev. 144, 439 (1966).

to eight neighboring points. A CDC 3600 digital computer was used to solve the eight by eight determinants.

The corresponding slopes of the isochronals (differential isochronals) are plotted in Fig. 6 and 7, respectively. These differential curves were obtained by differentiating the seventh-order polynomial used in obtaining the isochronal curves. The features to be noted are: (1) The Stage III region shows three distinct annealing processes consisting of one main peak ($T^C \approx -45^\circ\text{C}$) and two small peaks preceding it ($T^B \approx -93^\circ\text{C}$). These peaks will be called, hereafter, peaks "A", "B", and "C" starting from lower-temperature side. (2) The peak temperature for peak C, T^C shifts to lower temperature with higher damage. (3) The amount of recovery in Stage "C" is roughly proportional to the damage introduced at liquid-nitrogen temperature. In Stage "B" the recovery is roughly constant, but it increases with the background impurity content.

C. Isothermal Annealing

Isothermal annealing was carried out at temperatures successively 20°C apart from -130 to 75°C. Four

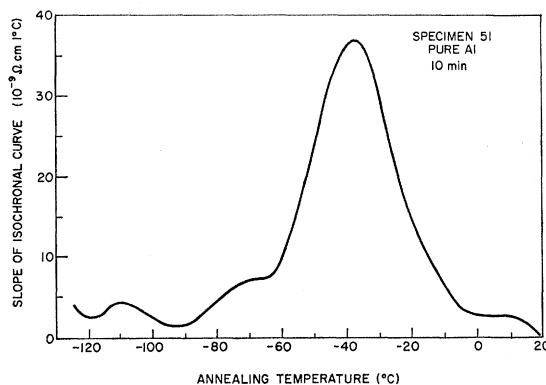


FIG. 6. Slope of isochronal recovery curve for specimen (5-1) pure Al irradiated with electrons near 80°K and annealed for 10 min every 10°C.

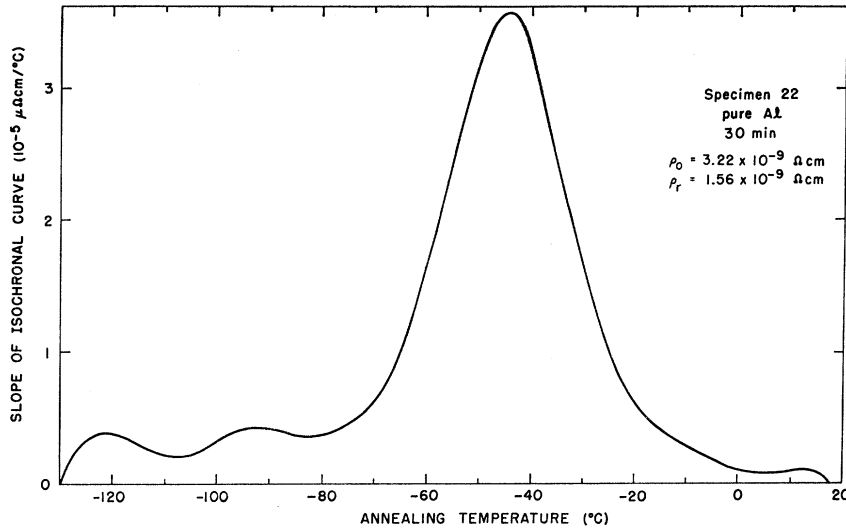


FIG. 7. Slope of isochronal recovery curve for specimen (2-2) pure Al irradiated with electrons near 80°K, and annealed for 30 min every 10°C.

specimen blocks containing seven specimens of pure Al, were given this treatment. At each temperature the residual resistivity remaining at liquid-helium temperature was measured after 4, 8, 16, 32, and 64 min of total annealing time. The temperature rise in the dummy specimen was recorded in each case and the annealing times were corrected. The correction time is normally less than 15 sec. Although the correction time depends on the apparent activation energy at each annealing step, errors from the use of the wrong activation energy are less than 1 sec.

These results are shown in Figs. 8 through 14. Each graph consists of stepwise isothermal anneals for the individual specimen. The activation energies associated

with Stage III region were obtained for each step of anneal using the following relation (slope method):

$$\left(\frac{d\rho}{dt}\right)_1 / \left(\frac{d\rho}{dt}\right)_2 = \exp\left\{-\frac{E}{k}\left(\frac{1}{T_1} - \frac{1}{T_2}\right)\right\}, \quad (1)$$

where ρ is the defect resistivity, T_1 and T_2 are the two annealing temperatures, and t is time.

It is to be noted that the apparent activation energies for the regions of the peaks "A," "B," and "C" have different values. From these isothermals, isochronal curves were constructed as shown in Fig. 15, where the total annealing time at each temperature is 64 min and 20°C annealing steps. These curves are to be compared

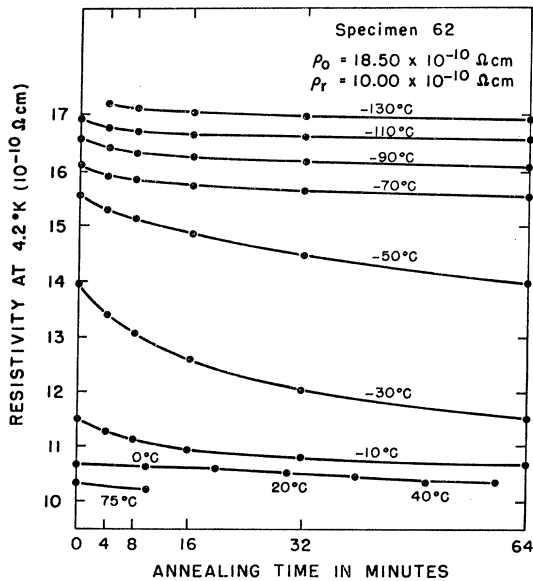


FIG. 8. Isothermal annealing of the electrical resistivity increase ($\Delta\rho$) between -130 and 75°C for specimen (6-1) pure Al following electron irradiation near 80°K.

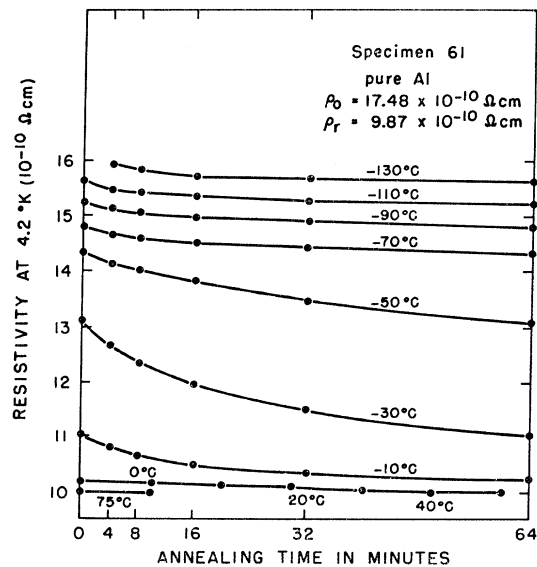


FIG. 9. Isothermal annealing of the electrical resistivity increase ($\Delta\rho$) between -130 and 75°C for specimen (6-2) pure Al following electron irradiation near 80°K.

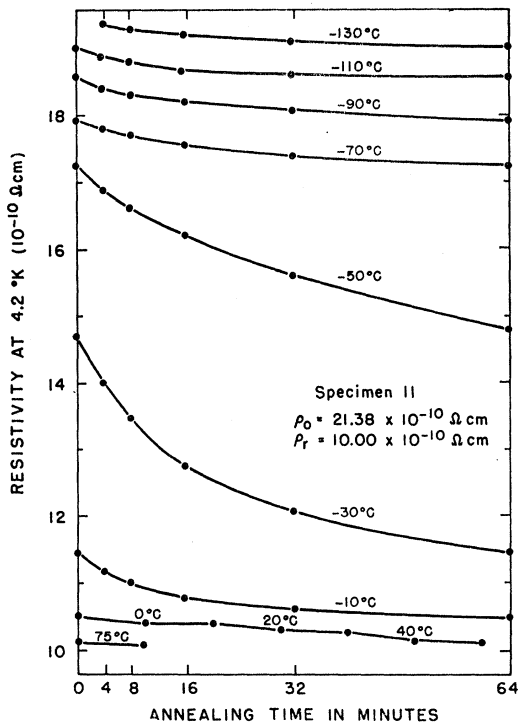


FIG. 10. Isothermal annealing of the electrical resistivity increase ($\Delta\rho$) between -130 and 75°C for specimen (1-1) pure Al following electron irradiation near 80°K .

with the isochronals (10 min, 30 min, and 10°C step) discussed previously.

The main features of these results are summarized below.

(1) The recovery rate is gradual from -130 to -70°C and followed by a rapid annealing process in the temperature range from -70 to -10°C , which corresponds to main peak "C" mentioned before.

(2) This rapid annealing seems to indicate peak "C" is caused by a recovery process governed by one mechanism with an average activation energy $E_{\text{III}} = 0.63 \pm 0.04$ eV.

(3) Apparently there is no change of activation energy with a change in the background impurity content in pure Al.

(4) Above the peak "C" region (~ 0 to 75°C) the recovery is almost 100%; no additional annealing peaks were observed in this region.

(5) Isochronals constructed from isothermal curves are remarkably similar to the isochronals of 10 min, 30 min every 10°C . The shifting of peak "C" to lower temperature with higher dose can be observed in Fig. 15 for pure Al.

D. Isothermal Annealing (Alternate Temperature)

Two irradiated pure Al specimens mounted on the same block were annealed at alternate temperatures of -40°C and -50°C . The results are plotted in Fig. 16.

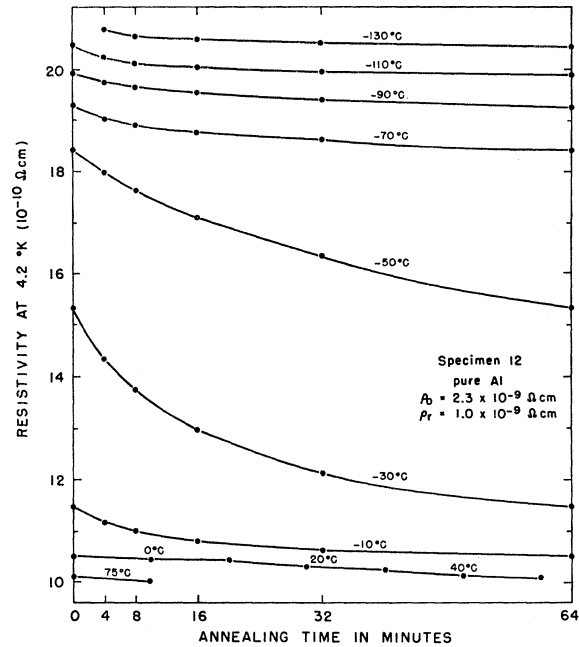


FIG. 11. Isothermal annealing of the electrical resistivity increase ($\Delta\rho$) between -130 and 75°C for specimen (1-2) pure Al following electron irradiation near 80°K .

Slope change method was used to determine the activation energy for the recovery process in Stage III. The average activation energy is found to be $E_{\text{III}} = 0.61 \pm 0.03$ eV. This value is in agreement with the value obtained in the previous section (also by the slope change method). The difference in activation energies

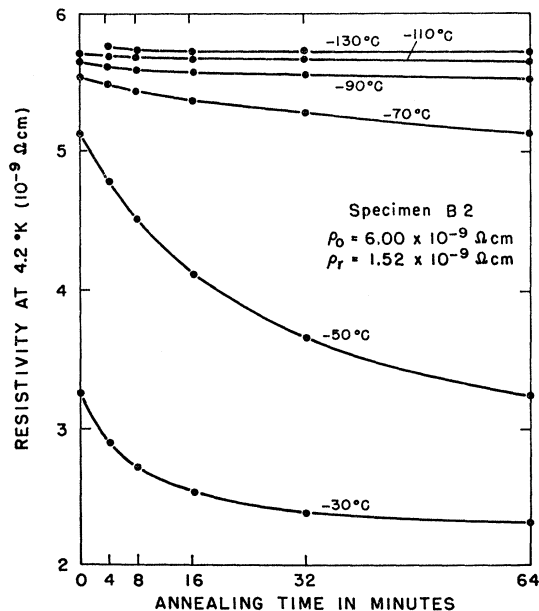


FIG. 12. Isothermal annealing of the electrical resistivity increase ($\Delta\rho$) between -130 and 75°C for specimen (B-1) pure Al following electron irradiation near 80°K .

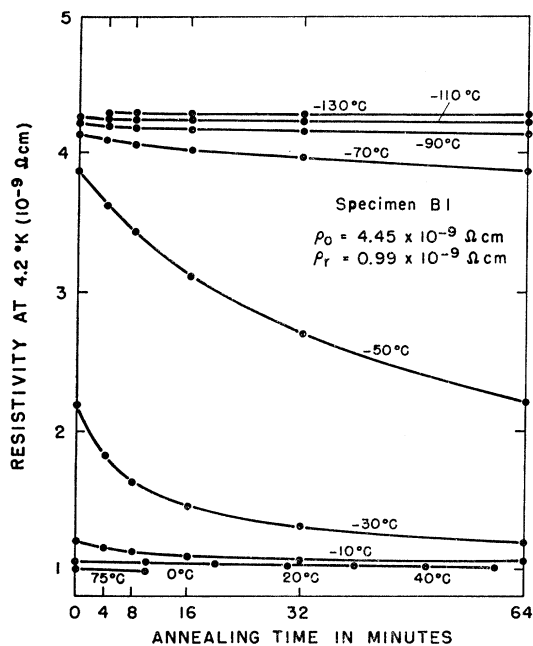


FIG. 13. Isothermal annealing of the electrical resistivity increase ($\Delta\rho$) between -130 and 75°C for specimen (B-2), pure Al following electron irradiation near 80°K .

determined from a sudden temperature change of -50 to -40°C and -40 to -50°C was within the experimental error.

E. Determination of the Activation Energy Spectrum

The annealing of kinetic processes distributed in activation energy has been discussed in detail by Primak.¹⁴

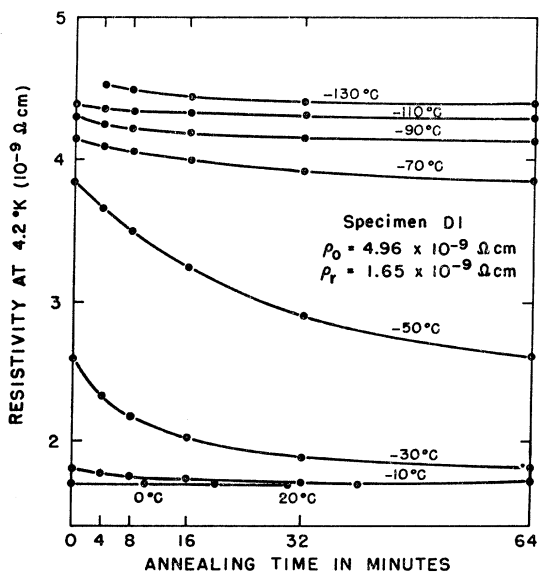


FIG. 14. Isothermal annealing of the electrical resistivity increase ($\Delta\rho$) between -130 and 75°C for specimen (D-1) pure Al following electron irradiation near 80°K .

¹⁴ W. Primak, Phys. Rev. **100**, 1677 (1955); J. Appl. Phys. **31**, 1524 (1960).

The calculation of activation energy spectra for first-order processes have been carried out by Magnuson, Palmer, and Koehler,¹⁵ by Bredt,¹⁶ by Herschbach,¹⁷ and by Bauer *et al.*¹⁸ This method has been applied to second-order processes by Dworschak, Herschbach and Koehler.¹²

In the present paper work the activation energy spectra were determined under the following assumptions: (a) Independent processes are distributed in activation energy and (b) the frequency factor is constant.

The calculations were iterated until the change upon iteration of the amount annealing with energy between E and $E+dE$ was less than 1% of its value at any E . Values of the frequency factor B (for first-order) and of B/δ (for second-order processes), where $\delta/100$ is the resistivity associated with a defect concentration of 1%, were chosen in such a way that the isothermals taken at successively higher temperatures fit smoothly

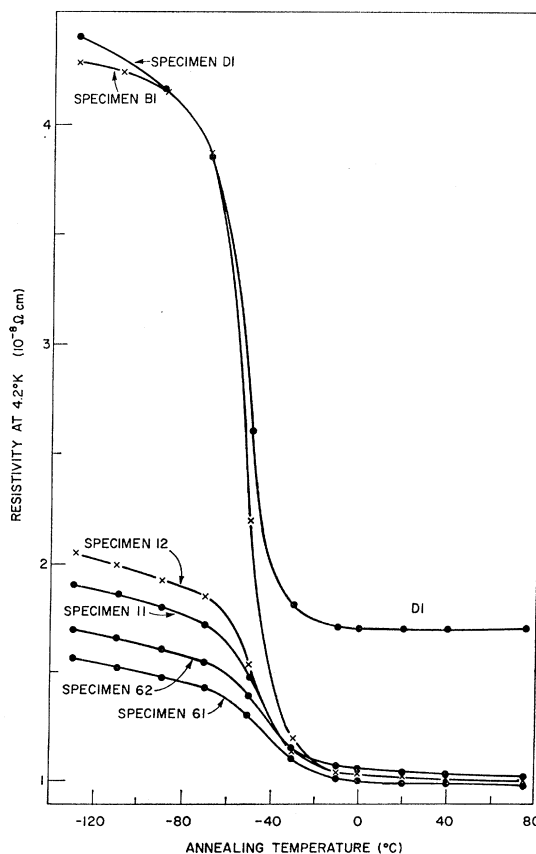


FIG. 15. Isochronal curves for pure Al specimens reconstructed from isothermal data of specimens (D-1, B-1, 1-2, 1-1, 6-2, 6-1).

¹⁵ G. D. Magnuson, W. Palmer, and J. S. Koehler, Phys. Rev. **109**, 1990 (1958).

¹⁶ J. H. Bredt, Ph.D. thesis, Urbana, Illinois, 1960 (unpublished).

¹⁷ K. Herschbach, Phys. Rev. **130**, 554 (1963).

¹⁸ W. Bauer, J. DeFord, J. S. Koehler, and J. W. Kauffman, Phys. Rev. **128**, 1497 (1962).

FIG. 16. Isothermal annealing at alternate temperatures of -40 and -50°C for pure Al specimen (7-1, 7-2) irradiated with electrons at near 80°K .

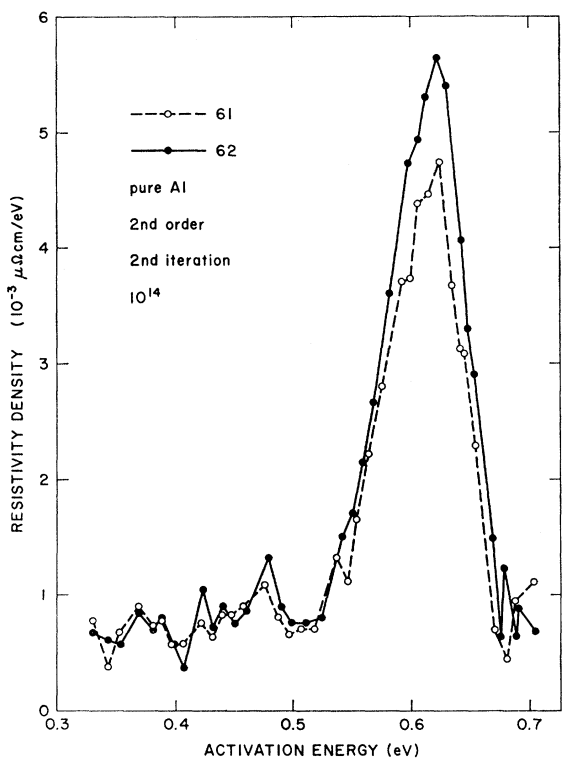
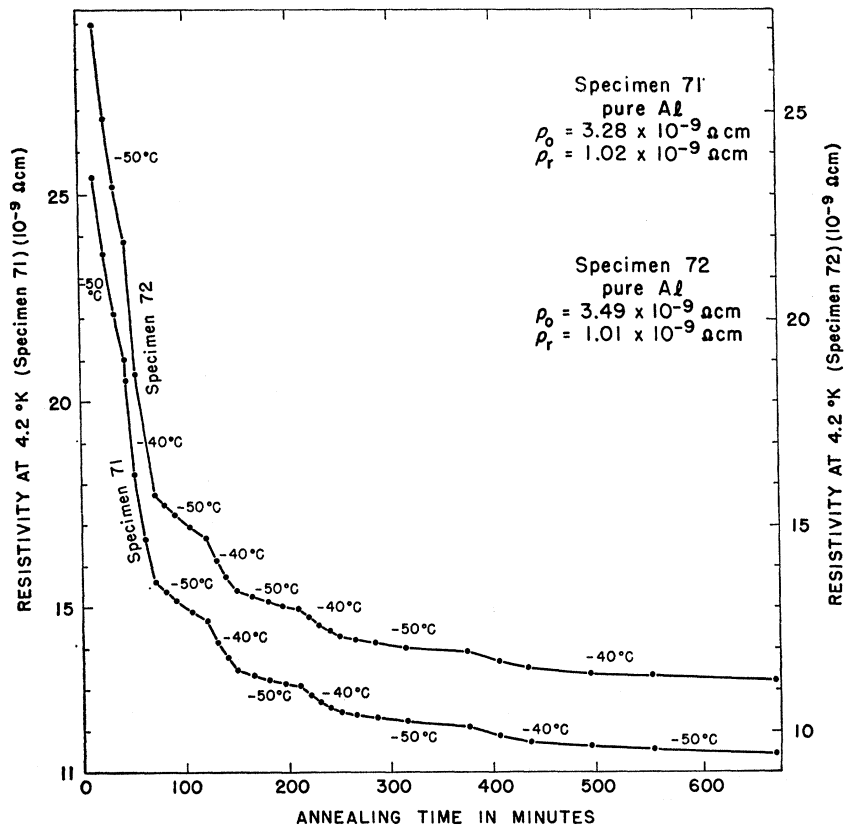


FIG. 17. Activation energy spectra for specimens (6-1, 6-2) pure Al. In Figs. 17-20 the 10^{14} is the frequency factor used. It is $B/\delta = 10^{14} \text{ eV}/\mu\Omega \text{ cm min} = 1.67 \times 10^{18} \text{ eV}/\Omega \text{ cm sec}$.

together. After the activation energy spectra were obtained, using these spectra, new activation energy spectra were calculated (second iteration).

F. Activation Energy Spectra

The activation energy spectra for pure Al are analyzed by the methods discussed in the previous section.

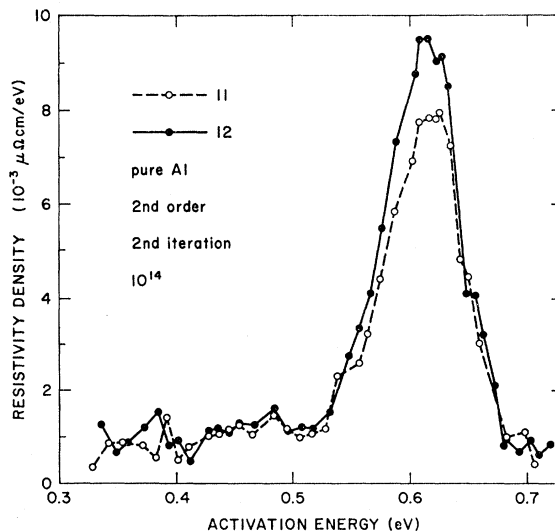


FIG. 18. Activation energy spectra for specimens (1-1, 1-2) pure Al.

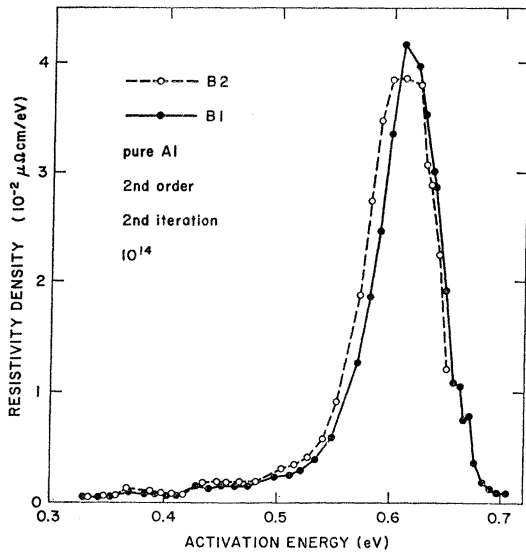


FIG. 19. Activation energy spectra for specimens (B-1, B-2) pure Al.

The spectra are shown in Fig. 17 through 20 for second-order kinetics. These spectra show structures similar to those observed in the differential curves of the isochronals. The following points should be noted:

(1) Two small peaks and a main peak corresponding to peaks *A*, *B*, and *C*, as mentioned in the isochronal annealing section, are again observed.

(2) Main peak "*C*" centers at about 0.60 ± 0.02 eV with the half-width of 0.06 ± 0.01 eV.

(3) Peaks "*A*" and "*B*" are found at about 0.38 eV and 0.46 eV respectively. The height of the peaks "*A*" and "*B*" remain roughly constant with dose.

(4) No other peak is observed above peak "*C*."

(5) The shape of the spectrum is similar to the typical differential isochronal curve of the pure Al for the case of frequency factor $B/\delta = 10^{14}$ eV/ $\mu\Omega$ cm min. The main peak symmetric about the center of the recovery region in Stage III. The position of the peak was found to be close to that of first-order kinetic treatment.

The spectra obtained using first-order kinetics are very similar to those obtained from second-order kinetics. It is not easy to decide which analysis should be used although we show below that peak *C* obeys second-order annealing kinetics.

G. Determination of the Order of Kinetics

To determine the kinetics of the State III peak *C*, two samples of pure Al were isothermally annealed at -50°C for 500 min, and the decrease of resistivity with time was followed by taking the specimens out of the annealing bath and measuring the resistivity at liquid-helium temperature.

This isothermal data was then fitted to second-order

kinetics as described by the kinetic equation

$$1/(\rho_t - \rho_\infty) - 1/(\rho_0 - \rho_\infty) = \alpha t, \quad (2)$$

with

$$\alpha = (\sigma \nu A / \delta) e^{-E/kT}, \quad (3)$$

where ρ_0 , ρ_t , and ρ_∞ are the resistivities at the beginning of the anneal, at a general time t , and after an infinite time, respectively; A is the entropy factor, ν is the frequency factor, σ is the capture volume in atomic volumes, E is the activation energy, T is the absolute temperature δ is the resistivity associated with the defects which are annihilated, and k is Boltzmann's constant.

The best fit to the data was obtained by least square method and a CDC 3600 digital computer was used. The results are given in Fig. 21. The data lie on a straight line in each case, and show that the over-all kinetics of the Stage III *C* is second order.

IV. DISCUSSION

A. Activation Energy

If the migration of a certain defect is a thermally activated process with a single energy of activation E , the rate of annealing of this defect at temperature T ($^\circ\text{K}$) is generally expected to follow an equation of

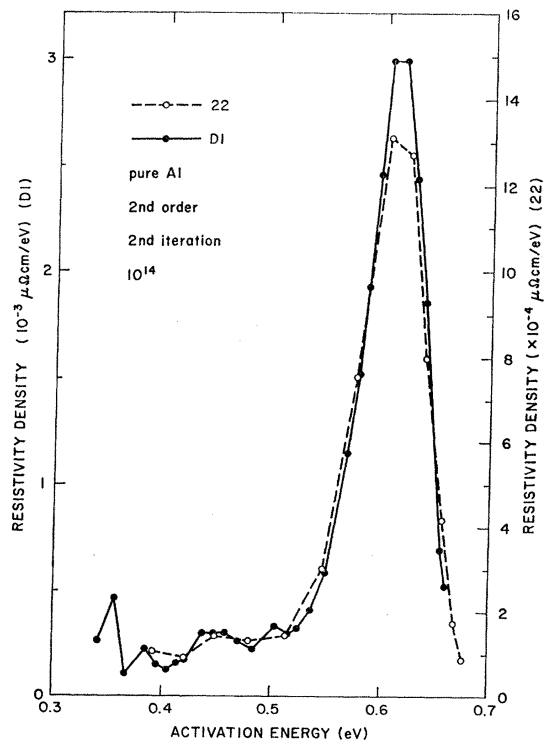


FIG. 20. Activation energy spectrum for specimen (D-1) pure Al.

the form^{19,20}

$$-dn/dt = f(n, q_1, q_2, \dots, q_n) \exp(-E/kT), \quad (4)$$

where n is the defect concentration and the q 's represent properties of the specimen leading to defect annihilation (e.g., spatial distribution of sinks), t is the time, T the temperature, k Boltzmann's constant, and E the activation energy.

If the associated increase in electrical resistivity $\Delta\rho$ is a single-valued function of n , which is a reasonable assumption for n sufficiently small, then it follows that

$$\left(\frac{d(\Delta\rho)}{dt}\right)_1 / \left(\frac{d(\Delta\rho)}{dt}\right)_2 = \exp\left\{-\frac{E}{k}\left(\frac{1}{T_1} - \frac{1}{T_2}\right)\right\}. \quad (5)$$

The activation energy for Stage III C of pure Al as determined by (a) the slope change method described above in isothermals at successively higher temperature and isothermal annealing between alternate temperatures, and (b) from the analysis of the activation energy spectra, is $E_{III}^c = 0.62 \pm 0.04$ eV.

In an earlier work of electron irradiation in pure Al Sosin *et al.*⁸ reported an activation energy of $E_{III}^c = 0.448 \pm 0.009$ eV, using the method of Meechan and Brinkman.²⁰ This value is considerably lower than the value obtained in the present work. This large discrepancy is probably due to the method of analysis. The determination of activation energy E by the Meechan-Brinkman method requires both isothermal and isochronal annealing data for initially identical specimens, with the relation²⁰

$$\ln \Delta t_i = \text{const} - E/kT_i, \quad (6)$$

where Δt_i is the increment of isothermal annealing time required to produce the same property change increment as was observed in the i th isochronal annealing pulse at T_i .

In this method, as they have clearly stated in their original paper,²⁰ they assume that the spatial distribution of sinks is constant or is only a function of the defect concentration. This may not be the case in Stage III annealing. The resistivity remaining after a long anneal at an annealing temperature is not only a function of defect concentration, but is also a function of the annealing temperature. This may be the reason that the apparent activation energy determined by the Meechan-Brinkman method is lower than that found in the present work.

B. Number of Jumps and Capture Volume

One common difficulty that all existing models face in explaining Stage III annealing is the low number of jumps found experimentally in Stage III. These

¹⁹ A. N. Lowan, N. Davids, and A. Leveson, *Bull. Am. Math. Soc.* **48**, 739 (1942).

²⁰ C. J. Meechan and J. A. Brinkman, *Phys. Rev.* **103**, 1193 (1956).

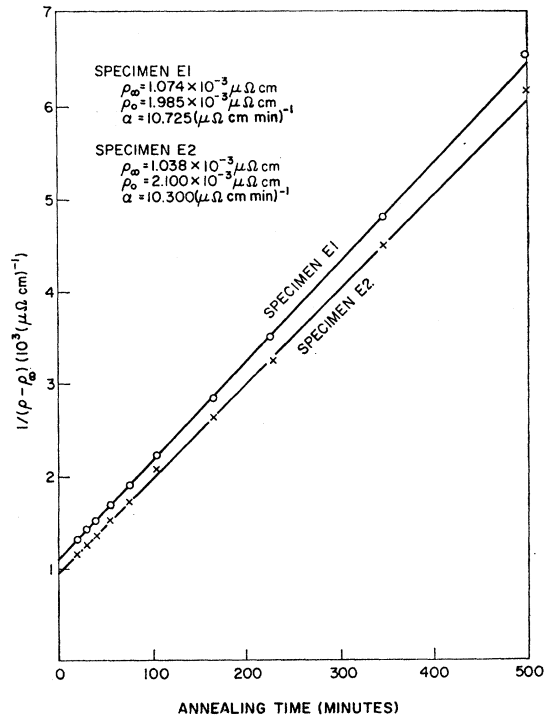


FIG. 21. Long isothermal annealing of electron-irradiated pure Al. Two samples were isothermally annealed at -50°C for 500 min.

models (which will be discussed in later sections) predict a large number of jumps for the process responsible, since a long range migration mechanism is associated with it.

The number of jumps required to anneal out half the damage is given by

$$n_j = A \nu t_{1/2} e^{-E/kT}, \quad (7)$$

where $t_{1/2}$ is the time for the resistivity to halve during a particular isothermal anneal. This number can be determined from our experimental data, taking $\nu A \cong 1.5 \times 10^{14} \text{ sec}^{-1}$ and $t_{1/2} = 30$ min in the case of $T = 223^\circ\text{K}$. This gives a value of $n_j = 3.4 \times 10^8$ for $E = 0.62$ eV.

The predicted number of jumps depends on the model and the mechanism of the recovery process. However, for (1) vacancy model, (2) divacancy model, (3) interstitial model, and (4) migration of di-interstitial model, the predicted number of jumps is of the order of c^{-1} where c is the concentration of defects. This concentration in the present experiment is of the order 10^{-5} , which predicts a number of jumps to be 10^5 . This approximate calculation shows a discrepancy between the measured and the predicted number of jumps.

This discrepancy is also observed in electron irradiation of pure Al by Sosin *et al.*⁸ if the present value of activation energy $E = 0.62$ eV is used.

From the data obtained after neutron irradiation of

pure Al by Federighi *et al.*¹ the jump frequency calculated is about 10^8 which is small compared with the predicted number of jumps.

One way to understand this discrepancy is to assume that the defects are uniformly spread, but that the recombination occurs with a large "capture volume", the defect migration will be random but less than $1/c$ jumps will be required for annihilation. For the present case the concentration is of the order of 10^{-5} and we then require a capture volume, $\sigma = 1/n_j c$ where σ is measured in atomic volumes.

This gives a capture volume of the order 30 atomic volumes.

The capture volume can also be determined from the long isothermal annealing data. The main peak "C" in Stage III was found to obey the over-all second-order kinetics, as shown in Fig. 21. The second-order kinetics is described by the equation

$$1/(\rho_t - \rho_\infty) - 1/(\rho_0 - \rho_\infty) = \alpha t, \quad (2)$$

where

$$\alpha = (\sigma \nu A / \delta) e^{-E/kT}. \quad (3)$$

All the symbols in the above equation have been defined in the previous section. From the experimental isothermal annealing data given in Fig. 21 one gets $\alpha = 10.73$ ($\mu\Omega$ cm min)⁻¹ and $\alpha = 10.30$ ($\mu(\Omega$ cm min)⁻¹. $T = 223^\circ\text{K}$, $E = 0.62$ eV and the assumed value for δ of 2×10^{-4} Ω cm. These values give $\sigma \nu A = 3.6 \times 10^{15}$. Taking $\nu A \cong 1.5 \times 10^{14}$ sec⁻¹, the capture volume is of the order of 24 which agrees well with the other determination.

C. Temperature Width in Isochronal Annealing

For a recovery process which is singly activated with a unique activation energy E , the width of recovery temperature can be estimated as follows.²¹

If an annealing is carried out with a constant heating rate $T = \alpha t$, the rate of recovery of a physical property p which is proportional to the defect concentration c can be expressed as

$$-dp/dt = k_0 p^\gamma \exp(-E/kT), \quad (8)$$

where k_0 is a constant and γ is the order of kinetics.

For $\gamma = 1$ (first-order kinetics), the peak width at half-maximum ΔT is given by²²

$$\Delta T \cong 2.5[k(T_a)^2/E], \quad (9)$$

where T_a is the temperature at which the annealing peak occurs.

For $\gamma = 2$ (second-order kinetics), the width is approximated by²³

$$\Delta T \cong (8/3)k(T_a)^2/E. \quad (10)$$

²¹ G. J. Dienes and G. H. Vineyard, *Radiation Effects in Solids* (Interscience Publishers, Inc., New York, 1957).

²² R. O. Simmons, J. S. Koehler, and R. W. Balluffi, in *Symposium on Radiation Damage in Solids and Reactor Materials*, Vienna, 1962 (International Atomic Energy Agency, Vienna, 1963), p. 156.

²³ V. Vand, Proc. Phys. Soc. (London) A55, 222 (1943).

Higher-order kinetics can be analyzed in a similar way yielding similar results. In such cases it is found that peak width ΔT increases somewhat with the order of kinetics.

Using an activation energy $E = 0.62$ eV and peak temperature of $T_a = 228^\circ\text{K}$, the peak width is second order $\Delta T = 19.3^\circ\text{C}$, first order $\Delta T = 18.1^\circ\text{C}$.

Experimentally, in the present work, the peak width is found to be $\Delta T \cong 28^\circ\text{C}$ in pure Al.

This temperature broadening is probably due to the spread in the activation energy spectrum. In Figs. 17 through 20 the calculated half width of the activation energy peak observed in Stage III^c is 0.06 eV. Such a spread is more than enough to account for the extra width of the isochronal peak since a 10°K shift in peak position corresponds to a change of 0.03 eV in activation energy. It is possible that the spread in activation energy arises from the interaction between the migrating vacancy and the interstitial clusters which act as sinks. This same interaction gives rise to a capture volume such that once the vacancy is within this volume its annihilation is certain.

The major experimental results found in this experiment are as follows: Stage III in pure Al consists of a main peak "C" at about -45°C . There are two smaller distinct peaks "A" and "B" which are located on the low-temperature side of the main peak. Stage III C in pure Al obeys over-all second-order kinetics with an activation energy of $E_{\text{III}^c} = 0.62 \pm 0.04$ eV.

The most significant result of the present investigation is that the activation energy $E_{\text{III}^c} = 0.62 \pm 0.04$ eV for pure Al obtained differs from the earlier work of electron irradiation by Sosin *et al.*,⁸ who obtained $E_{\text{III}^c} = 0.45 \pm 0.01$ eV. The low activation energy they have obtained is believed to be due to their method of analysis for which they used the Meehan-Brinkman method. The present value of activation energy is in good agreement with the value obtained by neutron irradiation work.

The present research provides additional data which supports Federighi's¹⁻⁴ contention that vacancies migrate to give the annealing which occurs in Stage III. The activation energy observed in quenched aluminum by Doyama and Koehler²⁴ and by Zamboni and Federighi²⁵ agrees well with the Stage III migration energy found here and also with the values observed by Federighi,¹⁻⁴ and by Frois and Dimitrov.^{5,6} We therefore conclude that Stage III annealing in pure aluminum occurs by the migration of lattice vacancies. The annealing occurs at a somewhat lower temperature in the electron-irradiated specimens than in quenched samples because of the difference in the sink density.

²⁴ M. Doyama and J. S. Koehler, Phys. Rev. 134, A522 (1964).

²⁵ L. Zamboni and T. Federighi, (unpublished). The principal results are given in the paper by T. Federighi, in *Lattice Defects in Quenched Metals*, edited by R. M. J. Cotterill, M. Doyama, J. J. Jackson, and M. Meshii (Academic Press Inc., New York, 1965), p. 217.

ACKNOWLEDGMENTS

Two of the authors (Y. N. L. and M. D.) wish to thank O. C. Simpson for his interest and encouragement throughout the work. One of the authors (Y. N. L.) expresses thanks to the Associated Midwest Universities for the support he received during the tenure of a Thesis Appointment in the Solid State Science Division of

Argonne National Laboratory. The authors thank Duane Larson and Choochon Lee for their invaluable assistance throughout the experiment. It is also a pleasure to acknowledge the patient and helpful work of W. A. Schooley, Mike Mason, and Brad Clymer, the members of the Van de Graff accelerator crew of the Material Research Laboratory at the University of Illinois.

Magnetic Breakdown and Oscillatory Magnetoresistance by a Kubo Formula

W. G. CHAMBERS

Mathematics Department, Westfield College, London, N. W. 3, England

(Received 10 May 1967; revised manuscript received 11 August 1967)

Pippard's effective-path method for calculating the conductivity in a breakdown network is extended by the use of a Kubo formula. It is shown how to calculate oscillations of the conductivity with frequencies in H^{-1} corresponding to (a) the lens orbits in the hexagonal network for Mg and Zn, and (b) the area of the Brillouin zone of the hexagonal network. At fields much greater than the breakdown field, the lens oscillations in the two-dimensional system have the same amplitude as the average conductivity. A rough calculation suggests that in magnesium the lens oscillations should have a magnitude comparable with the triangle oscillations at high fields. The calculations made for the "zone" oscillations are very crude, but it seems quite likely that they are observable.

1. INTRODUCTION

THE discovery of magnetic breakdown¹ has required some modifications in the usual theories of the de Haas-van Alphen effect and of the magnetoresistance. Pippard^{2,3} has discussed the consequences of breakdown in terms of network models and the author has attempted to justify this approach in terms of a nearly-free-electron model⁴ and in terms of the theory of the effective Hamiltonian.⁵ A modified theory of the de Haas-van Alphen effect was developed by Falicov and Stachowiak⁶ in terms of a time-dependent Green's function and a similar theory was later developed by the author in terms of a time-independent Green's function.^{4,5} Both approaches treat the Green's function as a propagator on a Pippard network.

Falicov and Sievert⁷ developed a theory for the magnetoresistance using a Pippard network and the method of Chamber's path integral. Another method was developed by Pippard,⁸ which is very simple and powerful when the relaxation caused by impurities and phonons can be neglected. This is called the "effective-

path" method. This technique was applied by Falicov, Pippard and Sievert⁹ to explain the remarkable oscillations observed by Stark¹⁰ in magnesium and zinc when the magnetic field was aligned along the hexad axis. It has also been applied by Young to explain oscillations in the magnetoresistance observed in tin.¹¹

In the case of magnesium and zinc the relevant Pippard network is a hexagonal system of coupled orbits as shown in Fig. 1. The triangles (at K) are very small, and they appear to be responsible for the oscillations. Phase coherence within these triangles was fully taken into account, but it was assumed that phase coherence on the longer arms could be neglected. In consequence the triangles acted as three-way scatterers which came into resonance whenever the magnetic field was such that a Landau level for the triangular orbit was at the Fermi energy. But further experiments by Stark¹² have also detected oscillations caused by the lens orbits, and to explain this it would appear to be necessary to develop a theory which can take phase coherence into account to a higher degree.

The purpose of this paper is to develop such a theory. It is based on the Pippard effective-path method, but this method is extended by the use of a Kubo formula for the conductivity. In order to apply this theory

¹ M. H. Cohen and L. M. Falicov, *Phys. Rev. Letters* **7**, 231 (1961).

² A. B. Pippard, *Proc. Roy. Soc. (London)* **A270**, 1 (1962).

³ A. B. Pippard, *Phil. Trans. Roy. Soc. (London)* **A256**, 317 (1964).

⁴ W. G. Chambers, *Phys. Rev.* **140**, A135 (1965).

⁵ W. G. Chambers, *Phys. Rev.* **149**, 493 (1966).

⁶ L. M. Falicov and H. Stachowiak, *Phys. Rev.* **147**, 505 (1966).

⁷ L. M. Falicov and P. R. Sievert, *Phys. Rev.* **138**, A88 (1965).

⁸ A. B. Pippard, *Proc. Roy. Soc. (London)* **A287**, 165 (1965).

⁹ L. M. Falicov, A. B. Pippard, and P. R. Sievert, *Phys. Rev.* **151**, 498 (1966).

¹⁰ R. W. Stark (to be published).

¹¹ R. C. Young, *Phys. Rev.* **152**, 659 (1966).

¹² R. W. Stark (to be published).